Astron. Astrophys. 313, 591–604 (1996)

ASTRONOMY AND ASTROPHYSICS

On collimated stellar jet magnetospheres

II. Dynamical structure of collimating wind flows

Christian Fendt[1,2] **and Max Camenzind**[2]

[1] Lund Observatory, Box 43, S-22100 Lund, Sweden
[2] Landessternwarte Königstuhl, D-69117 Heidelberg, Germany

Received 28 September / Accepted 27 January 1996

Abstract. Outflows driven by rapidly rotating magnetospheres occur in various astrophysical systems. Of particular importance are stellar magnetospheres in close contact with surrounding accretion disks. This work continues the investigations of paper I, where the overall structure of the resulting magnetic surfaces has been calculated. Here, we investigate the dynamics of the wind flow in such collimated magnetospheres.

Since for most configurations the plasma pressure is unimportant, the relativistic cold wind equation is solved along various magnetic flux surfaces, providing in this way a two–dimensional mapping of the plasma velocity, density and energy. These parameters are discussed as a function of the magnetization σ that is a measure of the mass load in the magnetosphere. High magnetization means low–density magnetospheres, low magnetization high–density outflows.

For a magnetization constant across the magnetic surfaces, the asymptotic jet velocity increases and the particle density decreases with increasing distance from the jet axis. An increasing magnetization, on the other hand, leads to a plasma velocity decreasing and a density increasing towards the jet boundary. Collimated outflows are therefore expected to have inhomogeneous density and velocity profiles.

In the cold wind approximation the initial magnetization of the flow is the only parameter that determines the asymptotic velocity and density. For low magnetizations, $\sigma < 1$, velocity and density are found to behave as a power law in σ, while the fast magnetosonic Mach-number virtually stays constant at a value of 2.5. Flows, which are collimated into a cylindrical shape, convert twice as much of the Poynting flux into kinetic energy when compared to a monopole type outflow.

In distinction to previous models we find that the Alfvén surface and the surface of the fast magnetosonic points converge asymptotically to cylindrical surfaces parallel to the jet axis. This divides up the collimated jet into three separate regions: in the innermost part, the plasma flow remains sub–Alfvénic, in the middle super–Alfvénic, but sub–magnetosonic and, only in the outer part, jet plasma flows super–magnetosonically. Applications for the jet structure of protostellar outflows are discussed.

Key words: magnetohydrodynamics – ISM: jets and outflows – stars: pre-main-sequence – stars: magnetic field – stars: mass loss – stars: neutron

1. Introduction

In a previous paper (Fendt et al. 1995, hereafter paper I) we calculate the global structure of a collimating jet magnetosphere originating in a magnetized star-disk system. The relativistic, force-free Grad-Schlüter-Shafranov equation describing the 2D local force-balance was solved under model assumptions related to a star-disk-jet system. We mainly concentrated on the YSO scenario since galactic (stellar) jets are predominantly observed in the case of protostellar sources such as T Tauri stars or embedded IR sources. The model underlying the numerical calculations was introduced in its original form by Camenzind (1990) and further extended to a stellar wind topology (Fendt 1994, paper I).

However, in paper I we only briefly considered the dynamics of the plasma motion in the collimating jet magnetosphere.

This topic will be addressed in the present paper. In particular, we are interested in the dependency of the dynamical parameters of the plasma flow on the magnetization and its 2D structure across the jet. The plasma motion is treated as a stationary, axisymmetric, magnetized cold wind originating near the stellar surface and is described by the wind equation. The underlying field structure is not self-similar and includes special relativity. The magnetosphere guiding the plasma is collimated from a stellar dipole to an asymptotically cylindrical structure resembling the small opening angles observed for protostellar jets. In principle, however, the results represent a magnetic field distribution with the *global* topology of any star-disk-jet scenario.

Send offprint requests to: C. Fendt (Lund Observatory)

The self-consistent back reaction of the plasma's inertia with the magnetic field is not included in the solutions presented here and will be subject of our future work. We will discuss the validity of this approach and estimate the deviations from the (unknown) self-consistent solution.

However, the solutions of the wind equation are exact solutions for any given magnetic flux surface. Therefore, the results presented in this paper could generally be applied to any magnetized, highly collimated wind flow.

We believe that as long as the jet boundary remains fixed, the magnetic field structure does not essentially change by variations in the magnetization. Our aim was *not* to treat the collimation process itself.

Since the fundamental work of Weber & Davis (1967) the problem of stationary, axisymmetric, magnetohydrodynamic (MHD) wind flows was further developed by various authors. Special relativistic cold winds were investigated by Michel (1969) and Okamoto (1978). Goldreich & Julian (1970) and Kennel et al. (1983) further included gas pressure. Camenzind (1986) formulated the wind equation in the context of general relativity. The key step toward the treatment of the two–dimensional problem was first made by Blandford & Payne (1982) in the case of self–similar cold disk winds.

The 2D problem is essentially more difficult to solve. The force-balance across the field depends on dynamical parameters of the wind flow, which are not known a priory. In fact, the long standing problem of a self-consistent solution for collimating magnetospheres, together with appropriate global boundary conditions, is still not being fully solved.

Until now, further simplifications of the problem have to be made and most of the authors treating the local force-balance follow Blandford and Payne assuming self-similarity (Pelletier & Pudritz 1992, Contopoulos & Lovelace 1994, Contopoulos 1994, Rosso & Pelletier 1994, Tsinganos & Sauty 1992, Sauty & Tsinganos 1994, Ferreira & Pelletier 1995). Self-similarity, however, imposes problems near the jet axis and the solutions extend to infinity rather than being confined within a finite outer jet radius. Also, the observed star-disk-jet topology is barely self-similar.

Solutions that supersede the self-similar assumptions have been considered by Sakurai (1985, 1987) and Li (1993a,b). The Newtonian solutions of Sakurai collimate from an initially monopole type distribution, but just on a logarithmic scale. In the relativistic solutions presented by Li a fast collimation is already prescribed. The topology of both solutions does not correspond to a magnetized star-disk-jet scenario, observed for jet sources.

In comparison to these results we make a new approach. We leave the self-similarity assumption and prescribe the field structure solely using boundary conditions: a stellar dipolar magnetosphere, an accretion disk and an asymptotic cylindrically collimated jet. In the very next step, the wind solutions presented in this paper have to be considered for the cross-field force-balance in order to iteratively approach the self-consistent solution.

The structure of the paper is as follows. In Sect. 2 we introduce the fundamental equations connected with magnetized wind flows. We will briefly recall the basic equations from paper I. Sect. 3 contains a critical discussion about the possible influence of non self-consistency on the results. Our numerical results are presented in Sect. 4. We will discuss solutions to the cold wind equation with different dynamical parameters and along different flux surfaces in the jet.

An overview of numerical methods involved in the calculations can be found in Appendix B.

Throughout the present paper we apply the same notation as in paper I.

2. Stationary, axisymmetric MHD wind flows

Under the assumptions of stationarity, axisymmetry and a high plasma conductivity the local magnetohydrodynamic (MHD) force-equilibrium can be described by two basic equations governing the force-balance across the magnetic field (the Grad-Schlüter-Shafranov equation, hereafter GSS equation) and along the field (the wind equation), respectively. The structure of the magnetosphere follows from solutions of the GSS equation, while the dynamics of the wind motion results from the solution of the wind equation.

Since the calculation of the magnetosphere was the main subject of paper I, here we just briefly review a few basic properties of the GSS equation. The wind equation will be discussed in more detail.

2.1. *Simplifying assumptions*

Using $B \sim B_\star (r_\star/r)^2$ as an estimate for the stellar magnetic field, the ratio between gravitational and the Lorentz force could be expressed as

$$\Delta_{\rm G} = \left| \nabla \frac{GM_\star}{r} \right| \frac{4\pi\, n\, m}{|(\nabla \wedge \mathbf{B}) \wedge \mathbf{B}|} \simeq \frac{\dot{M}_{\rm jet} G M_\star}{r_\star^3 B_\star^2 v_{\rm P}} (r/r_\star). \qquad (1)$$

with the particle density n, the proton mass m and the poloidal wind velocity $v_{\rm P}$. For protostellar jets, $B_\star \sim 1000\,{\rm G}$, $\dot{M}_{\rm jet} = 10^{-9} M_\odot\,{\rm yr}^{-1}$, and we obtain $\Delta_{\rm G} \simeq 2\,10^{-2}\,(10\,{\rm km\,s^{-1}}/v_{\rm P})$ at a radius $r = 10\,R_\star$, or $\Delta_{\rm G} \simeq 5\,10^{-2}\,(400\,{\rm km\,s^{-1}}/v_{\rm P})$ at $r = 1000\,R_\star$, respectively. We therefore neglect the gravitational term for the wind motion.

Similarly, for the ratio between gas pressure and Lorentz force (or, equivalently, thermal energy and magnetic energy) we estimate the value of the plasma–beta

$$\Delta_{\rm P} = \frac{4\pi\,|\nabla P|}{|(\nabla \wedge \mathbf{B}) \wedge \mathbf{B}|} \simeq \frac{4\pi\, P}{B^2} \simeq \frac{2\,\dot{M}_{\rm jet}}{m\, v_{\rm P}} \frac{k_{\rm B}\, T}{B_\star^2 r_\star^2} (r/r_\star)^2\,. \qquad (2)$$

With typical protostellar parameters $\Delta_{\rm P} \simeq 2.6\,10^{-7}\,(T/10^4{\rm K})\,(r/R_\star)^2 (10\,{\rm km\,s^{-1}}/v_{\rm P})$. Thus, the cold wind assumption is reasonable. Neglecting the thermal pressure implies that the plasma velocity greatly exceeds the speed of sound. Numerical calculations of hot winds from T Tauri stars were performed by Paatz & Camenzind (1995).

The assumption of a cold wind greatly simplifies the wind equation since the slow magnetosonic critical point disappears.

Since in this paper the primary goal is the wind motion itself rather than the mass injection mechanism, the cold wind scenario is an acceptable assumption. For stellar jet sources, which are stronger magnetized than protostars, the preceding estimates are even more valid.

2.2. Conserved quantities

With the assumption of axisymmetry the magnetic field structure can be described by the magnetic flux function $\Psi(R, Z)$ measuring the magnetic flux passing a circle of radius R,

$$\Psi = \frac{1}{2\pi} \int \boldsymbol{B}_{\rm P} \cdot d\boldsymbol{A}, \qquad R\boldsymbol{B}_{\rm P} = \nabla\Psi \wedge e_\phi, \tag{3}$$

where $\boldsymbol{B}_{\rm P}$ denotes the poloidal magnetic field.

Ideal MHD (i.e. for a highly conductive plasma) implies mass conservation along Ψ. The plasma is moving only parallel to the flux surfaces. The mass flow rate per flux surface, $\eta = \eta(\Psi)$, is conserved. We define $\eta(\Psi)$ via the total mass flow rate,

$$\begin{aligned} \dot{M}(\Psi) &= m \int n\,\gamma \boldsymbol{v}_{\rm P} \cdot d\boldsymbol{A} = m \int \eta \boldsymbol{B}_{\rm P} \cdot d\boldsymbol{A} \\ &= 2\pi\, m \int_0^\Psi \eta(\Psi) d\Psi\,, \end{aligned} \tag{4}$$

with the particle (proton) mass m. $\boldsymbol{v}_{\rm P}$ denotes the poloidal plasma velocity and γ the Lorentz factor (see also Sect. 2.4 below). Therefore, $d\dot{M}/d\Psi \sim \eta(\Psi)$.

Each field line (flux surface) is rigidly rotating (Ferraro's law of isorotation), and thus the angular velocity of the field line is conserved, $\Omega_{\rm F} = \Omega_{\rm F}(\Psi)$.

With stationarity and axisymmetry, conservation laws for the total energy, E, and the angular momentum, L are associated. Because of the ideal MHD assumption these constants of motion are functions of the flux surface Ψ alone, $E = E(\Psi)$, $L = L(\Psi)$. Following Camenzind (1986) we write the conservation laws as

$$E(\Psi) = \mu\gamma - \frac{RB_\phi}{4\pi\eta}\Omega_{\rm F}\,, \tag{5}$$

$$L(\Psi) = \frac{1}{c^2}\mu\gamma R^2\Omega - \frac{RB_\phi}{4\pi\eta}\,. \tag{6}$$

μ denotes the plasma enthalpy, Ω the angular velocity of the plasma, γ the bulk Lorentz factor of the plasma and B_ϕ the toroidal magnetic field, respectively. In the cold wind limit, the enthalpy reduces to a constant, $\mu = m\,c^2$.

Both quantities E and L consist of a kinetic part and a magnetic part. Plasma is accelerated by conversion of electromagnetic energy (Poynting flux) into kinetic energy by Lorentz forces. Evidently, in a highly magnetized plasma the magnetic energy provides a rich energy reservoir per particle. Thus, such flows are expected to be accelerated generally to higher velocities.

Using the normalization

$$\begin{aligned} R, Z &\Leftrightarrow R_{\rm L}\,x, R_{\rm L}\,z\,, \\ \Psi &\Leftrightarrow \Psi_{\rm max}\,\Psi\,, \\ RB_\phi &\Leftrightarrow (\Psi_{\rm max}/R_{\rm L})\,T\,, \\ E, L &\Leftrightarrow \mu\,E, \mu\,L\,, \end{aligned}$$

where $R_{\rm L} = c/\Omega_{\rm F}$ denotes the light cylinder (LC) of the rigidly rotating magnetosphere ($\Omega_{\rm F}(\Psi) = $ const.) and $\Psi_{\rm max}$ the maximum magnetic flux, the conservation laws (5) and (6) can be rewritten in dimensionless form as

$$E(\Psi) = \gamma - \sigma\,T\,, \tag{7}$$

$$L(\Psi) = \frac{1}{\Omega_{\rm F}}\left(\gamma x^2\Omega - \sigma\,T\right)\,. \tag{8}$$

The magnetization parameter, σ, quantifies the magnetic flux in terms of the mass flux (Michel 1969),

$$\sigma(\Psi) = \frac{\Psi_{\rm max}\,c}{4\pi\mu\eta(\Psi)\,R_{\rm L}^2}\,. \tag{9}$$

Assuming a power law, $\eta(\Psi) \sim \Psi^n$, we can estimate σ in terms of the total mass loss rate in the jet,

$$\sigma(1) = 3\,10^{-8}\,\left(\frac{\dot{M}_{\rm jet}}{10^{-9} M_\odot {\rm yr}^{-1}}\right)^{-1} R_{\rm L,15}^{-2}\;\Psi_{\rm max,25}^2\,, \tag{10}$$

for e.g. a protostellar jet.

Throughout the following we will use normalized quantities only.

2.3. Structure of the jet magnetosphere

Ampère's law, rewritten in terms of the magnetic flux function Ψ, yields the GSS equation. Here, for the reason of legibility, we repeat the normalized, modified GSS equation from paper I,

$$\begin{aligned} x\nabla\cdot\left(\frac{D}{x^2}\nabla\Psi\right) &= -\frac{1}{\sigma^2}\frac{\gamma x}{M^2}\left(E' - \Omega\,L'\right) \\ &\quad -\frac{1}{x}\left(T^2 + M^2|\nabla\Psi|^2\right)(\ln\sigma)'\,, \end{aligned} \tag{11}$$

and its force-free version,

$$x\nabla\cdot\left(\frac{D}{x^2}\nabla\Psi\right) = -\,g_{\rm I}\,\frac{1}{x}\,I\,I'\,. \tag{12}$$

where the term D is defined as $D = 1 - M^2 - x^2$ (in Eq. (11)) or $D = 1 - x^2$ (in Eq. (12)), respectively. The $'$ indicates the derivative $\partial/\partial\Psi$. The normalized poloidal current is defined as

$$I(\Psi)\,I_{\rm max} \equiv \int \boldsymbol{j}_{\rm P} \cdot d\boldsymbol{A}\,. \tag{13}$$

The relativistic Alfvén Mach-number M is given by

$$M^2 = \frac{4\pi\mu\eta^2}{n}\,, \tag{14}$$

with the proper particle density n.

The normalized quantities T and I are related via $T^2 = g_{\rm I}\,I^2$. With the normalization of the equations (11) and (12), certain

coupling constants are introduced, expressing the strength of the GSS operator (l.h.s. in Eqs. (11) or (12)) in terms of the source current (i.e. the r.h.s. in Eqs. (11) or (12)). The coupling constant in the force-free limit is

$$g_{\rm I} = \frac{P^2 I_{\rm max}^2}{\pi^2 \Psi_{\rm max}^2} = 2.7 \left(\frac{I_{\rm max}}{10^{11}{\rm A}}\right)^2 \left(\frac{P}{2^{\rm d}}\right)^2 \Psi_{\rm max,25}^{-2}, \quad (15)$$

with the rotational period P of the field or the central star, respectively (numerical values for a protostellar jet).

As can be seen in Eq. (11), the source term, with the dimension of a reduced toroidal current density, is non-linear and depends on various functions, which are unknown *a priori*. These functions describe the dynamical state of the plasma motion and have to be calculated from the wind equation (which, however, requires a prescription of the underlying magnetosphere). As a serious complication, the location of the magnetosonic surfaces are *not* known from the beginning (they, in turn, define the boundaries of the integration domain and impose certain boundary conditions).

Due to these difficulties, it is not yet possible to solve the problem without assuming further simplifications.

While other authors use e.g. self-similarity (Blandford & Payne 1982, Contopoulos 1994, Sauty & Tsinganos 1994), some other special scaling (Pudritz & Norman 1983, Pelletier & Pudritz 1992, Rosso & Pelletier 1994) or monopole type topologies (Sakurai 1985, 1987) for the magnetic field distribution, we applied a force-free ansatz for the GSS equation, i.e, we solved Eq. (12) (see paper I). As a major result of paper I, we found that the regularity condition along the Alfvén surface (which is equal to the LC in the force-free approach) determines the shape of the jet radius in the collimation region.

2.4. The wind equation

The stationary plasma motion along a flux surface is described by the wind equation. In the relativistic case it can be derived from the normalization of the 4–velocity,

$$u^\alpha \equiv \{u^t, \boldsymbol{u}\} \equiv \gamma\{1, v_{\rm R}/c, \Omega, v_{\rm Z}/c\}. \quad (16)$$

For the poloidal component, we get

$$u_{\rm P}^2 = \gamma^2 \left(1 - (x\Omega/\Omega_{\rm F})^2\right) - 1\,. \quad (17)$$

The toroidal velocity can be expressed in terms of the Alfvén Mach-number, the magnetization and the poloidal current,

$$u_\phi = \gamma x \Omega = \frac{1}{x}\sigma M^2 T + \gamma x\,. \quad (18)$$

The Lorentz factor γ and the angular velocity $\Omega = u^\phi/u^t$ have to satisfy the conservation of energy and angular momentum. Inserting the constants of motion, Eqs. (7), (8), into Eq. (17), together with the definition of the Alfvén radius,

$$x_{\rm A}^2 = \frac{\Omega_{\rm F} L}{E}\,, \quad (19)$$

provides the wind equation,

$$u_{\rm P}^2 + 1 = E^2 \frac{x^2(1 - M^2 - x_{\rm A}^2)^2 - (x^2(1 - x_{\rm A}^2) - x_{\rm A}^2 M^2)^2}{x^2(1 - M^2 - x^2)^2} \quad (20)$$

(Camenzind 1986). In the cold wind limit this equation simplifies to an implicit polynomial for the poloidal velocity of degree of 4

$$\sum_{m=0}^{4} A_m(x; E, L; \Phi, \sigma)\, u_{\rm P}^m = 0\,, \quad (21)$$

where the coefficients A_m depend explicitly on the magnetization σ, the flux tube function $\Phi = x\,|\nabla\Psi|$, and the flow parameters energy and angular momentum (Appendix A).

As a polynomial of 4th order, at each radius x the wind equation has 4 solutions $u_{{\rm P},i}(x)$, $(i = 1..4)$. We only take into account positive solutions, i.e. we consider the negative or complex solutions as "unphysical". Thus, there exist two *global* solution *branches* for the wind motion. Additionally, we require that the "physical" *global* wind motion passes the critical points smoothly (see next Sect.).

2.5. The critical wind solution

At the magnetosonic points the wind Eq. (20) becomes singular. A finite solution only exists if the nominator and the denominator vanishes together. Then, the poloidal plasma velocities at these critical points just equal the speed of the magnetosonic waves. As mentioned previously, neither the location of the critical surfaces nor the magnetosonic speed at this position is known *a priori*.

The global, critical solution of the wind equation is defined by a smooth transition of the plasma across the critical points. The derivative of the poloidal velocity along the field line must be finite. The physical interpretation is that, due to the stationarity assumption, shocks are not allowed in the plasma flow.

In principle, the derivative of the poloidal velocity, evaluated at the critical points, could be used as an additional condition for a critical solution. However, in our numerical approach (Appendix B.2), we do not solve for the derivatives. Instead, we investigate the local topology of the global wind solutions in the neighbourhood of the fast magnetosonic point.

We start with a solution for a carefully selected parameter set, and iteratively approach the critical solution by variation of the critical parameters. In the cold wind approach the critical parameter is the plasma energy $E(\Psi)$. For a weakly magnetized wind solution the energy has to be determined by this procedure with an accuracy of 10^{-9}!

The physical solution of the wind equation starts at zero velocity at the injection radius and passes, monotonically accelerating, the Alfvén point and the fast magnetosonic point.

We define the local fast magnetosonic Mach-number $M_F = (u_P/u_{FM})$ as the ratio of the relativistic poloidal flow velocity to the relativistic (fast) magnetosonic speed with

$$u_{FM}^2 = \frac{B_P^2}{4\pi\mu n}(1-x^2) + \frac{B_\phi^2}{4\pi\mu n}\,. \tag{22}$$

The corresponding magnetosonic wave propagates with u_{FM} in poloidal direction.

Since the fast magnetosonic point determines the critical solution, cold wind solutions with sub–Alfvénic or even sub–fast–magnetosonic asymptotic velocity are not uniquely defined by the energy parameter.

2.6. The role of the light cylinder

Special relativity is introduced due to the fast rotation of the stellar magnetosphere. As can be seen in Eq. (20), the LC is not a critical point of the wind motion. The plasma decouples from a rigid rotation with the magnetic field already at the Alfvén point (but still moves along the flux surfaces).

However, the poloidal Alfvén speed u_A becomes imaginary outside the LC,

$$u_A^2 = \frac{B_P^2}{4\pi\mu n}(1-x^2)\,. \tag{23}$$

Outside the LC, Alfvén waves can not propagate in meridional direction. Only fast magnetosonic waves are able to exchange information across the jet.

With the electric field perpendicular to the flux surface $E_\perp = x\,B_P$, Eq. (23) can be rewritten in terms of the electric field. This is a remarkable difference to the Newtonian MHD, where electric fields are generally negligible.

Note that Eq. (23) represents the poloidal Alfvén speed, Lorentz transformed from the corotating frame to the global frame,

$$u_A = (1/\gamma_v)\,u_{A,\mathrm{corotating}}, \tag{24}$$

with the Lorentz factor

$$\gamma_v = \left(1 - \left(\Omega_F R/c\right)^2\right)^{-1}. \tag{25}$$

3. Discussion of the present approach

As mentioned above, the magnetosphere underlying the wind motion was calculated using the force-free assumption. The self-consistent interaction between the plasma inertial forces and the magnetic field was not taken into account. However, for a field distribution prescribed, the plasma motion along a flux surface is determined exactly by the solution of the wind equation. The question is, whether and to which extent the force-free magnetosphere deviates from the self-consistent solution. The structure of the flux surfaces obviously influences the plasma motion.

For a highly magnetized plasma flow, $\sigma >> 1$, the back-reaction of the plasma inertia on the magnetic field is negligible. These solutions can be considered as quasi self-consistent despite the lack of an iteration procedure between the GSS and the wind equation.

In the case of weakly magnetized outflows, in particular in the case of protostellar jets, where the mean magnetization across the jet is $< 10^{-7}$, the plasma inertial forces may considerably deform the prescribed force-free field.

In the following we discuss the validity of our approach for low-σ flows.

3.1. Comparison to previous work

Blandford & Payne (1982) numerically found a relation between the initial opening angle of the flux surface, the specific angular momentum and the magnetization (defined, however, in a different manner) of the wind flow in their self-similar solutions.

Their Fig. 2 shows that for higher magnetizations (low κ in their paper), as long as the other parameters are kept fixed, the initial opening angle increases by 25° if the magnetization decreases by a factor of 100. For low magnetizations (particle dominated flows, $\kappa \geq 1$) the effect is becoming even less important.

Although their approach is quite different from ours, their result seems to indicate that inertia effects do not change the field structure heavily.

Sakurai (1985, 1987) calculated self-consistent, non self-similar solutions of the Newtonian GSS equation. His starting configuration for the iterative procedure is a purely radial field distribution, i.e. straight field lines in a monopole or split-monopole topology. The final self-consistent solution clearly collimates, but only on a logarithmic scale. The shape and position of the magnetosonic surfaces change, but not considerably and the strongest effect is near the z-axis.

In our view this clearly demonstrates that inertial forces change the field structure only slightly.

3.2. Strength of the total poloidal current

The total poloidal current enclosed by the jet can be estimated as follows. The toroidal field (and thus the poloidal current) can be derived from the conservation laws (7) and (8),

$$T = -\frac{E}{\sigma}\frac{x_A^2 - x^2}{1 - M^2 - x^2}\,. \tag{26}$$

For large radii $x_A^2 << x^2$ and $(1-x^2) << M^2$ and thus,

$$I\,I_{max} \simeq \frac{1}{2}\Omega_F \Psi_{max}\frac{\Phi}{u_P}\,. \tag{27}$$

In the force-free limit the inertial terms in Eq. (26) are neglected and we similarly derive

$$I_{max} = \frac{1}{2}\Omega_F \Psi_{max}\sqrt{g_I}\,. \tag{28}$$

Comparison between the maximum poloidal current in the force-free and non force-free case reveals

$$\frac{I_{max,ff}}{I_{max,nff}} = \sqrt{g_I}u_P\,. \tag{29}$$

This is a general result that does not depend on our model assumptions.

Would this increased poloidal current change the magnetic structure within the jet? If we compare the magnetic pressure gradient $I_{\rm max}^2 \nabla_\perp b_\phi^2$ with the magnetic tension by toroidal fields, $I_{\rm max}^2\, b_\phi^2\, \nabla_\perp x/x$, we see that both terms scale with the same factor, $I_{\rm max}^2$. Therefore the field distribution within the jet should not change with different strength of the poloidal current.

The external toroidal field, created by $I_{\rm max}^2$, will certainly compress the jet structure. It will affect the collimation process and will presumably change the asymptotic jet radius. However, since the asymptotic jet radius remains fixed in our solutions, the external field does not influence the solution presented here (we do not intend to treat the collimation mechanism itself). The local force equilibrium will not change drastically as long as the global boundary conditions remain fixed.

3.3. Source term in the GSS equations

A low magnetization suggests a very high coupling $\sim \sigma^{-2}$ of the source term in the GSS Eq. (11). We will now show that this is not true.

If we ignore the second source term of Eq. (11) (this is equivalent to the assumption of a constant magnetization across the flux surfaces) and compare Eq. (11) with Eq. (12), it follows

$$g_{\rm I}\, I\, I' = (1-x^2)\nabla\Psi\cdot\nabla(\ln M^2) - \frac{1}{\sigma^2}\frac{\gamma x^2}{M^4}\left(E' - \Omega\, L'\right). \quad (30)$$

Because of the logarithm, the first term of the r.h.s. is of the order of unity as it is the force-free term on the l.h.s. The remaining term has to be calculated from 2D wind solutions, since it depends on derivatives perpendicular to Ψ. However, for low magnetizations, energy and angular momentum are only varying weakly. The derivatives are very small (see Fig. 6 below), and together with the very high Alfvén Mach-numbers they suppress a strong coupling.

The explicit numerical calculation reveals that this term rapidly drops from $\sim 10^3$ near the injection radius to ~ 1 near the asymptotic radius of the flux surface. Thus, for most part of the integration domain the non force-free source term is comparable to the force-free one.

Whether these estimates will hold within a self-consistent treatment, could only be seen from the self-consistent solution itself.

4. Numerical results and discussion

The wind solutions presented in this section are calculated along a collimating jet magnetosphere derived and discussed in detail in paper I. The prime signatures of this magnetic structure are summarized as follows:

- A stellar dipolar magnetosphere is asymptotically collimated to a force-free cylindrical jet.
- Closed field lines within the gap between the stellar surface and the inner edge of an accretion disk allow for ongoing magnetic accretion.
- The asymptotic jet radius is of the order of the light cylinder, here we use $R_{\rm jet} = 3R_{\rm L}$.
- The shape of the jet boundary $R_{\rm jet}(Z)$ is determined by the regularity condition at the LC and the poloidal current distribution across the jet. The initial opening angle of the jet is 65°. The field is rapidly collimated to the asymptotic jet radius.

This magnetic field distribution is shown in Fig. 1. For the investigation of the wind dynamics, we chose a certain set of nearly equidistant flux surfaces (Fig. 1a). The corresponding flux tube function $\Phi(x)$ for each surface is shown in Fig. 1b. In comparison, in a monopole field distribution $\Phi = \cos^2\alpha = $ const., where α is the slope angle of the flux surface.

For small radii, the stellar dipole becomes visible in the outer flux tubes: Φ strongly increases near the star and decreases again in the transition region between the dipole and the open field. At intermediate radii the flux surfaces show a nearly conical structure ($\Phi \simeq$ const). As the flux tubes open up beyond the LC, Φ decreases. Finally, the collimation of the fields leads to a narrowing of the flux tube and therefore Φ increases again.

In the following we will first consider the plasma motion along a single flux surface and then compare the wind solutions for different surfaces. All together, this finally provides a 2D picture of the wind dynamics.

We have chosen an injection radius $x_{\rm inj} = 0.01$ with $u_{\rm P}(x_{\rm inj}) = 0$. It turned out that the exact location of plasma injection influences the wind speed at larger distances only weakly. What is essential, is the fast, rigid rotation of the magnetosphere anchored in the stellar surface. Compared to a disk wind topology, where the foot points of the field lines rotate with Keplerian speed and are located beyond the corotation radius $x_{\rm cor}$, a higher "centrifugal potential" is available in order to initiate the wind acceleration,

$$\Omega_{\rm F}/\Omega_{\rm Kep} = (x_{\rm inj}/x_{\rm cor})^{3/2}. \quad (31)$$

4.1. Solutions along a single flux surface

In this section we examine the wind motion along a single flux surface. Arbitrarily, we have chosen the surface $\Psi = 0.726$, collimating to an asymptotic radius $x_\infty = 2.36$ in the outer part of the jet (indicated in Fig. 1 with circles).

Figs. 2 and 3 show a selected set of dynamical parameters of a wind flow with a high magnetization $\sigma = 10$ and a low σ-flow solution ($\sigma = 10^{-5}$), respectively.

The solutions clearly illustrate the interrelation between the shape of the flux tube function and the plasma acceleration. With increasing radius, the magnetic energy decreases, getting converted into kinetic energy of the plasma via Lorentz forces. As realized by other authors, the effect of opening up the flux tube is similar to a hydrodynamic nozzle (e.g. Camenzind 1987, Li 1993a).

4.1.1. Highly magnetized flows

As mentioned above, in the high-σ limit the wind solution can be considered as quasi self-consistent.

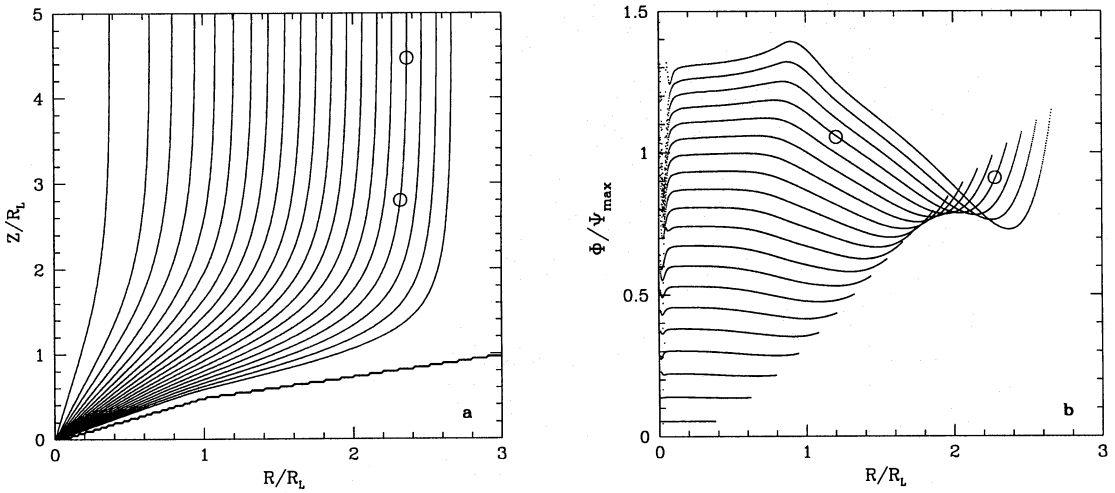

Fig. 1. a Magnetic flux surfaces $\Psi(x, z)$ (equivalent to solution AMP in paper I, Fig. 3a). The contours reflect the flux surfaces chosen for the wind solutions. The circles denote the magnetic flux surface used in the treatment in Sect. 4.1. Contour levels: .856 .813 .769 .726 .682 .639 .595 .551 .508 .464 .421 .377 .333 .290 .246 .203 .159 .115 .077 0.028. **b** corresponding flux tube functions $\Phi(x)$

The Alfvén point is located very close to the LC, $x_A = 0.98$. The Alfvén Mach-number reaches maximum values about ≤ 1.5. Note, that M is changed due to relativistic effects, $M(x_A) \neq 1$! Within $x \leq x_A$ the poloidal velocity increases approximately linear and the acceleration is only moderate compared to the region outside x_A.

However, we find that there is an upper limit on the magnetization, $\sigma \sim 10$. Beyond this, there exist no *global* solution branches extending to the asymptotic radius of the flux surface! Instead, the poloidal velocity reaches a maximum value at a certain radius and decreases again. There are only imaginary solutions to the wind polynomial beyond this radius.

The deceleration takes place until the poloidal velocity equals the magnetosonic speed again. Thus, the "endpoint" of the global stationary solution corresponds to a second fast–magnetosonic point along the flux surface. A deceleration below sub–magnetosonic velocities seems not to be possible.

Shocks may be expected at this position, violating the stationarity assumption. This might be an over-interpretation, but we mention that stationarity is directly connected with the energy parameter and thus with the fast magnetosonic point.

We believe that the deceleration is caused by the convergence of the the flux tubes near the asymptotic radius. Again, we recall the example of a hydrodynamic *de Laval* nozzle. In the hydromagnetic case the change of flux function $\Phi(x)$ plays the role of the change of size of the flow cross-sectional area in the hydrodynamic case (e.g. Li 1993a). A strong increase of $\Phi(x)$ (see Fig. 1) may lead to a deceleration of the plasma. The deceleration begins at the point where the rapid increase of $\Phi(x)$ sets in (Fig. 1b). Interestingly, in the hydrodynamic case a deceleration below sub-critical velocities is not possible in practice due to frictional forces.

Note that the preceding arguments are based on the assumption that the field structure remains fixed. In our approach it is given by the solution of the force-free GSS equation (see Sect. 3).

A plasma deceleration beyond the FM point is not controversial for MHD flows. The fast magnetosonic surface imposes a boundary condition for the GSS equation, which was not taken into account in our calculation in paper I. However, since the wind solution is nearly self-consistent for high-σ, one could interpret the flow behaviour such that it tries to 're-arrange' for the proper boundary condition for the force-free GSS solution. It seems that our GSS solution (with the chosen asymptotic boundary conditions) could not support cylindrical flows with $\sigma > 10$.

Any flux tube converges naturally as soon as its topology changes from a conical shape into a cylindrical shape (it would also converge in a fully self-consistent calculation). Therefore, a deceleration could be expected in any high-σ wind flow asymptotically collimating into a cylindrical shape and also in any re-collimating topology. Inclusion of thermal effects may change the fast magnetosonic speed slightly and this might be sufficient to shift the end point of the solution to the asymptotic radius. We will address this topic in a future work.

Finally, we mention an interesting feature visible in the toroidal velocity. The asymptotic ratio $u_P/u_\phi \simeq 0.4$ is rather high. We therefore conclude that the toroidal motion of the plasma in relativistic jets (with small jet radii in terms of the LC) may strongly increase the Doppler broadening of spectral lines.

Highly magnetized flows are expected to occur as relativistic winds and jets from compact objects (see also Sect. 4.1.3). However, there are only few galactic relativistic sources observed to date. One is the famous SS 433 jet, emanating from a neutron star in a high mass X-ray binary system (D'Odorico et al. 1991). More recently, Mirabel & Rodriguez (1994) discovered a superluminal ejection of radio condensations from the high energy source 1915+105, however, the nature of the source is not yet

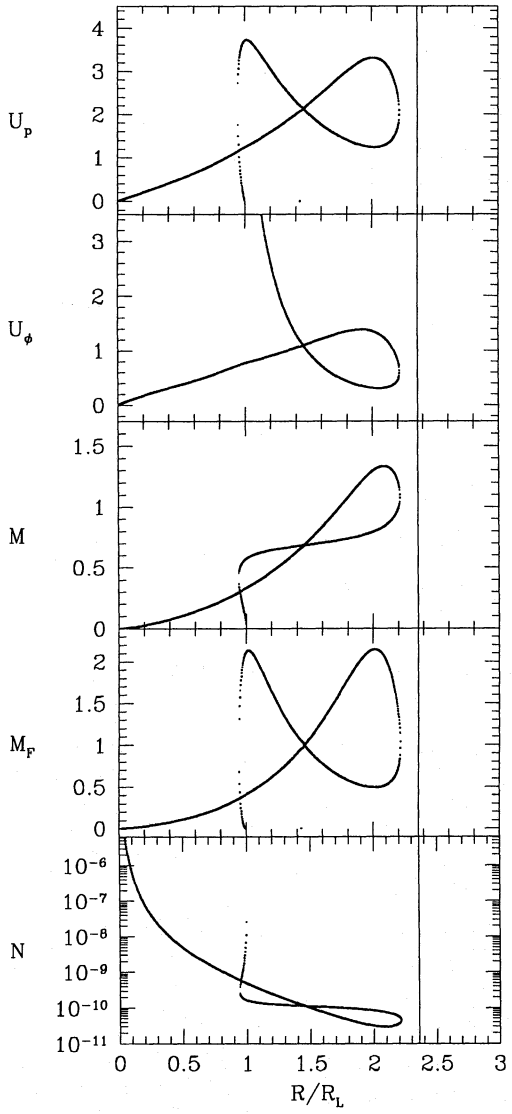

Fig. 2. Poloidal and toroidal wind velocities, u_P, u_ϕ (in units of c), Mach-numbers M and M_F, and particle density N (in cm^{-3}) of a wind solution of high magnetization $\sigma = 10$. These are solutions along the flux surface $\Psi = 0.726$. The vertical line indicates the asymptotic radius of the flux surface, $x_\infty = 2.36$. The asymptotic jet radius is at $x = 3$. The first intersection of the solution at $x = 0.98$ (which is absent in the u_ϕ-plot) indicates the Alfvén point, the second one at $x = 1.46$ the (fast) magnetosonic point of the flow, respectively

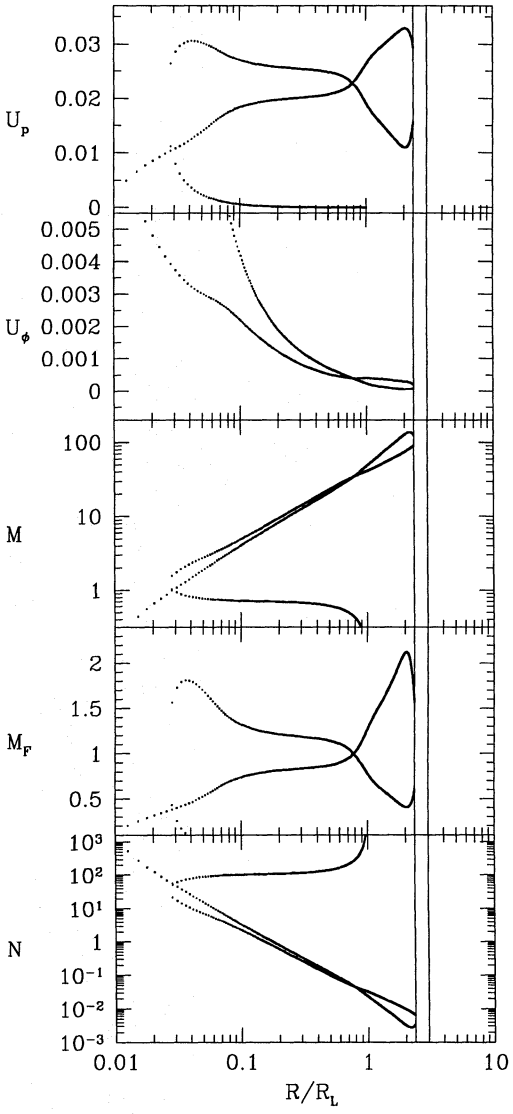

Fig. 3. The wind solution for a weakly magnetized flow, $\sigma = 10^{-5}$. Notation and units as in Fig. 2. Note the different scale of the abscissæ. The vertical lines indicate the asymptotic radius of the flux surface, $x_\infty = 2.36$, and the asymptotic jet radius, $x_{\rm jet} = 3$. The Alfvén point is located at $x = 0.019$, the (fast) magnetosonic point at $x = 0.78$, respectively

clearly known. Superluminal motions were also detected from the galactic X-ray source GRO J1655-40 (Tingay et al. 1995). Interestingly, the jet velocities are just the same in both sources, $0.92c$.

The problem here in modelling the jet *dynamics* is that some important parameters are quite uncertain. There is still some doubt about the driving source and parameters, as magnetic flux involved, rotational periods, or jet radii are just not known.

We just note that in our model (highly) relativistic jet velocities can indeed be obtained. A jet speed of $0.92c$ corresponds to $u_P = 2.35$ (if we neglect toroidal motion). This value is similar, but less than the maximum speed in the wind solution presented in Fig. 2. It fits nicely to our conclusion that the plasma can hardly be accelerated to higher speed in highly collimated jets due to the convergence of the flux tubes mentioned above. However, we do not like to argue too far, since some basic jet parameters are not known from the observations. In our model, the essential parameters are the scaling of the jet radius in terms of the injection radius and the rotational periods (equivalent to the position of the LC).

Galactic jet sources predominantly belong to the relatively numerous class of weakly magnetized protostellar jets (see section below). Even so, we emphasize that the protostellar jet mass loss rates are observed as a *mean* value across the jet diameter.

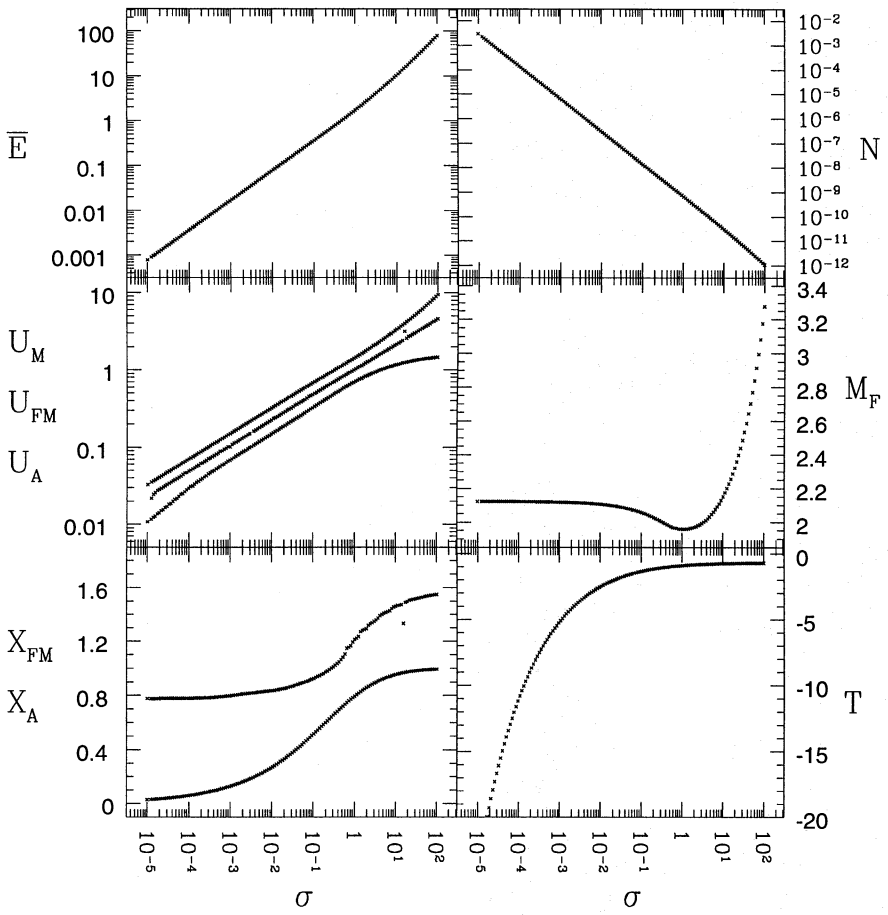

Fig. 4. Dynamical parameters as a function of the plasma magnetization. Calculated from the set of critical wind solutions to 149 different magnetization parameters σ along the magnetic flux surface $\Psi = 0.726$. Total energy minus rest energy, $\overline{E} = E(\Psi) - 1$, in units of the rest energy, mc^2. Maximum poloidal velocity near the asymptotic radius, u_M, poloidal velocity at the (fast) magnetosonic point, u_F and at the Alfvén point, u_A, respectively. Position of the (fast) magnetosonic point, x_{FM}, and the Alfvén point, x_A. Particle density N in cm^{-3} at the position of u_M. (Fast) magnetosonic Mach-number, M_F. Poloidal current, T, in units of Ψ_{max}/R_L

The distribution of the mass loss rate perpendicular to the jet axis is not known observationally. Depending on the mass injection mechanism, it would most likely vary across the jet by a large factor. Therefore, highly magnetized mass flow along certain flux surfaces could not be excluded in a protostellar jet. There are some models considering relativistic jets from young stars (Kundt 1993).

4.1.2. Weakly magnetized flows

Low magnetization plasma flows are observed as highly collimated jets emanating from young stellar objects. From observations, the magnetization of protostellar jets is of the order of $\sigma < 10^{-8}$. However, in the calculations we were not able to solve the wind equation in the case of such a weak magnetization. This is because in this case the Alfvén point is located within the *numerical* stellar radius (limited by the possible size of the finite elements). Here we show a wind solution with $\sigma = 10^{-5}$. We will see in the next section that it is possible to scale the numerical values by a simple power law.

In distinction to the high-σ case, now the wind solutions reach the asymptotic regime of the field line. The field is too weak compared to the plasma inertia in order to brake the flow efficiently.

The Alfvén radius is located $x = 0.02$, very close to the injection radius and well apart from the LC. Thus, the plasma "decouples" earlier from the field and the flow reaches high Alfvén Mach-numbers. The toroidal velocity fastly decreases to a value less than $\leq 1\%$ of the asymptotic poloidal velocity. The particle density changes by five orders of magnitude.

The plasma acceleration takes place predominantly at smaller radii. However, comparison to the high σ-flow reveals that the ratio

$$u_M : u_P(x_{FM}) : u_P(x_A) \simeq 3 : 2 : 1 \tag{32}$$

remains nearly unchanged. This has also been proven for other magnetizations (Fendt 1994).

The ratio of the kinetic energy to the magnetic energy of the plasma at the magnetosonic point is

$$\left(\frac{E_{kin}}{E_{mag}}\right) = \left(\frac{\gamma - 1}{E - \gamma}\right) \simeq 0.5\,. \tag{33}$$

This is a general correlation for low magnetization flows.

4.1.3. Magnetization and the asymptotic jet

In this section we show how the plasma dynamical parameters depend on the magnetization. Fig. 4 shows the parameters of

the critical wind solutions along the flux surface $\Psi = 0.726$, calculated for a set of 149 different numerical values of the magnetization σ.

The main result is that for a weak magnetization $\sigma \lesssim 1$, the maximum poloidal velocity $u_{\rm M}$ along a flux surface follows a power law,

$$u_{\rm M} = K\sigma^{1/3}\,, \tag{34}$$

with $K = 1.52$ for the flux surface considered. Similarly, the asymptotic proper particle density goes as $N = 6.3\,10^{-10}\,{\rm cm}^{-3}\,\sigma^{-4/3}$. The (fast) magnetosonic Mach-number, however, remains constant for weak magnetization,

$$M_{\rm F} \simeq 2.15\,. \tag{35}$$

The number values of the constants derived above depend on the choice of the flux surface. From previous work (Fendt 1994) we know that for a flux surface located farther outside, the maximum velocity as well as the magnetosonic Mach-number do *slightly* increase. But the overall picture remains the same. Note, that in the case of a monopole topology of the magnetic field the asymptotic velocity analytically derived is $u_{\rm M} = 1.0\,\sigma^{1/3}$ (Michel 1969). Thus, the collimated field accelerates the plasma more efficiently. The poloidal field curvature provides an additional accelerating force in poloidal direction due to the magnetic tension term in the Lorentz force.

Using the power laws derived we are able to extrapolate to lower magnetizations comparable to protostellar jets. With $\sigma \simeq 10^{-9}$ we calculate a typical protostellar jet velocity of $450\,{\rm km\,s}^{-1}$, in nice agreement with the observations. The particle density is about $600\,{\rm cm}^{-3}$ which differs by one order of magnitude from the observational value (derived using shock models for the jet knots, Mundt et al. 1987, 1990).

Interestingly, for the relativistic jet of SS 433, with a jet speed of $v = 0.26\,c$ (or $u_{\rm P} = 0.27$), the power law gives $\sigma = 6\,10^{-3}$, a value which is surprisingly small.

We believe that our results are rather general since the asymptotic wind motion does not depend on the field topology in the innermost regime at radii less than the injection radius. Additionally, the asymptotic parameters are not strongly influenced by the exact position of the injection radius.

Therefore, if we hypothetically assume some other system topology within the injection radius, the asymptotic wind solution would only differ slightly, as long as the jet parameters remain the same. This hypothetical jet source might be e.g. a neutron star or black hole disk-wind-magnetosphere.

4.1.4. Poloidal current and toroidal field

Now we investigate the total poloidal current *distribution* $T(x, z)$ as it results from the wind solution.

In the force-free limit the total poloidal current is conserved along the flux surface.

In the non force-free situation currents perpendicular to the flux surfaces are possible providing additional components of the Lorentz force. These forces, exerted on the plasma, will distort the force-free field configuration, until a new equilibrium state, described by the self–consistent solution, is achieved.

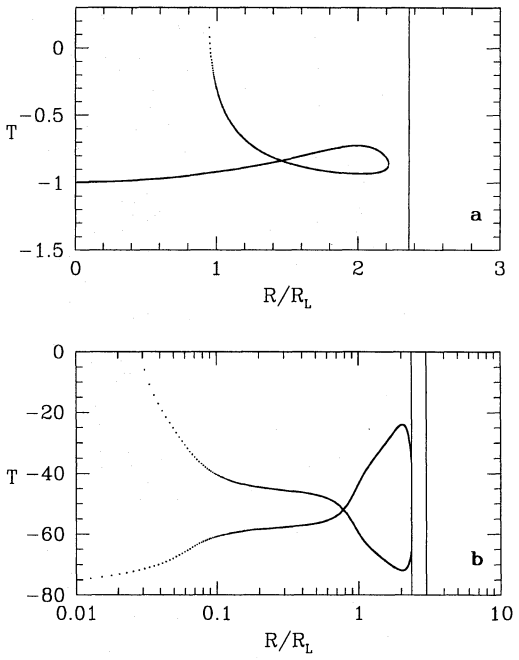

Fig. 5a and b. Poloidal current $T(x)$ in the wind solution along $\Psi = 0.726$. **a** Highly magnetized flow (see Fig. 2). **b** Weakly magnetized flow (see Fig. 3)

Fig. 5 shows the poloidal current strength $T = T(x;\Psi) = xB_\phi/\Psi_{\rm max}$ along the same flux surface as indicated in Fig. 1.

In the highly magnetized solution the poloidal current remains more or less constant, $T \simeq -0.8$. The numerical value is near the theoretical value given by the choice of current distribution for the force-free GSS equation, $T(\Psi = 0.726) = \sqrt{g_I}I(\Psi = 0.726) = 0.694$ (see paper I). This is consistent with a force–free magnetosphere and a quasi self–consistent solution for the wind equation.

In the weakly magnetized solution the poloidal current strength increases towards small radii by a factor of 4. Towards the asymptotic radius, the ratio between the low and high-σ solution current strength is about 30 times larger than in the high σ solution. With $u_{\rm M} = 0.037$ (see Fig. 3) and $g_I = 1.9$ this result nicely resembles the estimate Eq. (29).

For a discussion concerning the influence of the maximum current on the field structure we refer to Sect. 3.2.

4.2. Dynamical properties across the asymptotic jet

In order to achieve an information on the 2D velocity distribution, we calculated the wind parameters for a chosen set of different flux surfaces.

Since the magnetization remains a free parameter in the cold wind approximation, it is possible to choose different distributions for the magnetization across the flux surfaces, $\sigma(\Psi)$. This is equivalent to the assumption of different mass flow distributions in the jet.

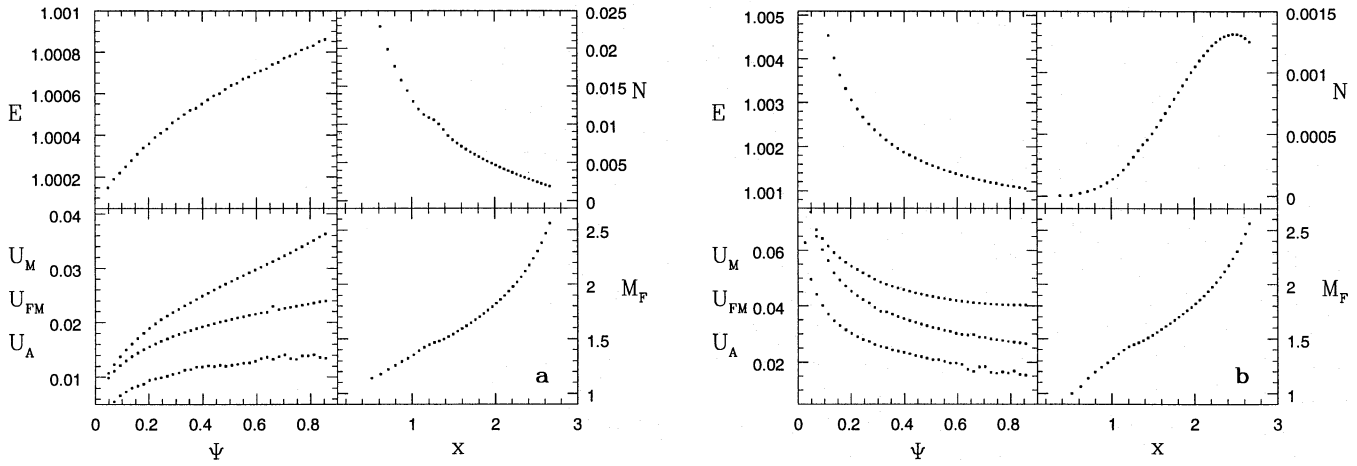

Fig. 6a and b. Dynamical parameters across the asymptotic jet, calculated from the critical wind solution along the flux surfaces shown in Fig. 1. **a** Assumption (36), **b** assumption (37). Notation as in Fig. 2.

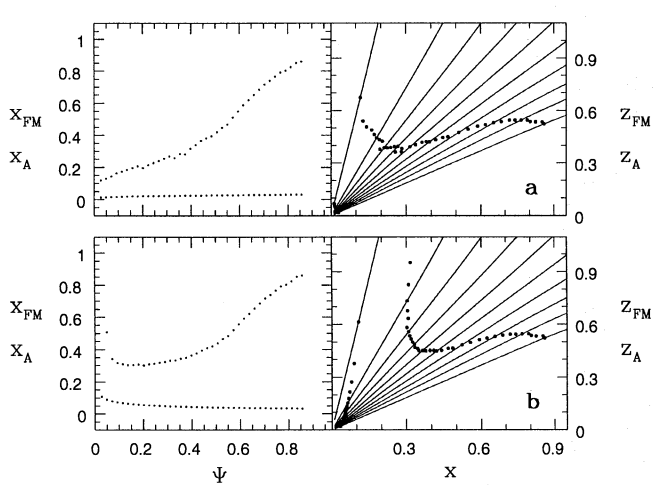

Fig. 7a and b. Position of the Alfvén radius (x_A, $z(x_A)$) and the (fast) magnetosonic point (x_{FM}, $z(x_{FM})$), as a function of the flux surface Ψ and 2 D shape of the critical surfaces (only a subset of the full integration domain is shown). **a** Assumption $\sigma(\Psi)$ = const. = 10^{-5}; **b** $\sigma(\Psi) = 10^{-5}\,\Psi^{-2}$.

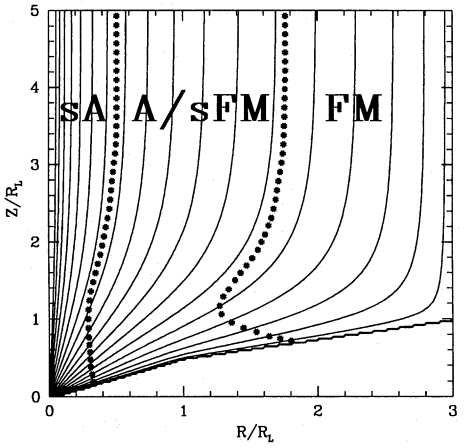

Fig. 8. The overall structure of the critical surfaces in a cylindrically collimated magnetic jet. In the asymptotic regime, they intend to run parallel to the flux surfaces, i.e. parallel to the jet axis. The meaning of the various regions is as follows: sA: sub–Alfvénic, A/sFM: super–Alfvénic, but sub–magnetosonic, FM: super–magnetosonic

Here, we show results for two different assumptions for the magnetization distribution,

$$\sigma(\Psi) = 10^{-5} = \text{const.}, \quad (36)$$

$$\sigma(\Psi) = 10^{-5}\Psi^{-2} \quad (37)$$

(for other examples see Fendt 1994). In both cases the flow is weakly magnetized. Assumption (36), a constant magnetization throughout the jet, is equivalent to a constant mass flow rate on each flux surface. Assumption (37) corresponds to a mass flow increasing towards the edge of the jet.

Our results are shown in Fig. 6. Each point in the figure refers to the *asymptotical* result of a critical wind solution for a single flux surface.

We see that, assumption (36) leads to a velocity distribution increasing with radius with a decreasing particle density. For assumption (37) the velocity decreases and the density increases, respectively. In both cases the magnetosonic Mach-number increases with radius. It can be seen that there must exist a single flux surface, where asymptotically $M_F = 1$. Within this flux surface the flow remains sub–magnetosonic, while outside it reaches super–magnetosonic velocities (in the next Sect. we will examine the structure of the magnetosonic surfaces).

Observationally, it is not yet possible to resolve the internal structure of (proto)stellar jets in such detail. However, it is well manifested that protostellar jets generally consist of various flow components. The high velocity components are always located near the jet axis, while the lower velocities are found towards the edge of the jet. Thus, our assumption (37) seems to be more reasonable.

However, we have to note that the observed data are literally interpreted either in an "entrainment scenario" , where the outermost jet regions interact with the ambient medium and thus, these jet layers become decelerated (Hartigan et al. 1993, Raymond et al. 1994), or in a two component disk-wind-stellar-wind model (Kwan & Tademaru 1988, Solf 1987, Böhm & Solf 1994). Our results provide an alternative explanation.

From the viewpoint of the plasma injection into the jet magnetosphere, a mass flow predominantly concentrated in the outer layer would naturally be expected. The injection of plasma near the jet axis (from the poles of the star) is clearly less efficient because of the large slope of these field lines. On the contrary, the acceleration along non-polar field lines is more effective. Additionally, Rayleigh-Taylor and Kelvin-Helmholtz instabilities may cause a mass transfer from the inner part of the accretion disk into the outer layers of the collimating magnetosphere.

Thus, observations of the velocity profile across the asymptotic jet would also provide an information about the innermost circumstellar region of the jet, which would never be possible to resolve. However, to date, the spatial resolution available is still too low in order to resolve a detailed velocity profile across a protostellar jet.

4.3. Position and shape of the critical surfaces

The shape and/or position of the critical surfaces is not known *a priori*. It depends on the structure of the magnetosphere as well as on the mass flow distribution and the plasma dynamics. It is this fact that makes the self-consistent treatment of the problem extremely difficult.

Since the magnetosonic Mach-number $M_{\rm F}$ is directly connected to the stability of magnetohydrodynamic jet flows (Appl & Camenzind 1992), it becomes important to know where the boundary between sub– and super–magnetosonic jet velocities is located.

In the previous work of Sakurai (1985, 1987) the critical surfaces were calculated to be circularly (or elliptically) shaped surfaces in a slowly collimating monopolar field structure. A similar (circular) topology of the Alfvén surface was computed by Sauty & Tsinganos (1994), using a self–similar ansatz for the magnetic field. In the very fast collimating (relativistic) jet magnetosphere of by Li (1993a,b) the critical surfaces close to innermost flux surface within a relatively short distance from the origin.

All these results imply that the jet flow is structured by the critical surfaces basically *along* the jet axis (i.e. with critical surfaces perpendicular to the jet axis).

Our results are somewhat different. We find that the critical surfaces turn asymptotically into a cylindrical shape, i.e. they structure the asymptotic jet flow *perpendicular* to the jet axis (Fig. 7).

Note that the shape of the magnetosonic surface is not affected by the LC. The radial position depends on the numerical value of the σ-parameter of the flow, while the shape of the surface is related to the $\sigma(\Psi)$-distribution across the jet.

In summary, we would like to propose an overall jet structure shown in Fig. 8: The critical surfaces divide the asymptotic jet into different regimes *across* the jet axis. In the outermost part the flow may reach super–magnetosonic velocities, while with decreasing *cylindrical* radius the plasma flow remains sub–magnetosonic or even sub–Alfvénic.

The magnetosonic structure of the jet does not necessarily mirror the true plasma velocity distribution. The poloidal velocity in the innermost, sub–magnetosonic regime along the axis may well supersede the velocity in the outer layers (see Fig. 6).

It should be emphasised that the result discussed above arises from the treatment of a *cold* wind. In principle, inclusion of internal pressure could affect the shape of the critical surfaces. A pressure gradient would support the acceleration of the plasma and change the speed of the magnetosonic waves. Indeed, the work by Sauty & Tsinganos (1994) also considers thermal effects.

A *slow* magnetosonic surface calculated for our field topology may be located at a finite distance from the star along the axis. Nevertheless, a negligible thermal pressure (see Eq. 2) would hardly affect the position of the Alfvén and fast magnetosonic surface.

Thus, the different shape of the critical surfaces seem to be due to the different *topology* of the solutions, i.e. the self-similarity assumption in the case of Sauty & Tsinganos.

5. Conclusions

In this work we investigated the dynamics of a cold plasma flow in a magnetic field structure collimating from a stellar dipolar field towards a cylindrical jet. The field structure was prescribed and was originally calculated and discussed in a previous paper. Within this field distribution we considered wind flows along different flux surfaces and with a different magnetization. Altogether, this provides a 2D picture of the plasma dynamics of stellar jets.

The magnetosphere underlying the wind motion was not yet calculated in a self-consistent way. However, we discussed the validity of the present approach and concluded that a large deviation from a self-consistent solution is unlikely. In any case, the wind solutions are exact solutions along a prescribed flux surface.

For highly magnetized flows we found that above a limiting value for the magnetization, $\sigma \lesssim 10$, no global, stationary wind solutions reaching the asymptotic jet do exist. Equivalently, this corresponds to an upper limit for the maximum poloidal jet speed, $u_{\rm P} = \gamma v_{\rm P}/c \lesssim 3$. At the endpoint of the stationary solutions, magnetohydrodynamic shocks may be expected. The jet speed observed for two highly relativistic, superluminal sources are just below this limit.

The low magnetization solutions extend up to the asymptotic regime of the flux surface. But even in this case, the plasma gets slightly decelerated before it reaches the asymptotic jet.

The relation between the magnetization and the asymptotic poloidal plasma velocity follows a power law. This relation is similar to that of monopole type field structures found by Michel

(1969), but increased by a certain factor, constant along the field line. For a flux surface in the outer part of the jet, this factor is of the order of 2. Thus, a collimated field distribution accelerates the wind twice as efficiently as a purely radial field.

Using the power law derived, we extrapolated our results to very low protostellar jet magnetizations. The derived asymptotic jet velocities of about 450 km s^{-1} nicely fit the observed values.

For low magnetizations the magnetosonic Mach-number is independent of the magnetization. Its constant value is of the order of 2.5 in the outer (super–magnetosonic) part of the jet. Since the fast magnetosonic Mach-number is known to be directly coupled with the growth rates of destabilising MHD modes, our result may be applied for stability calculations of (protostellar) jets.

The velocity distribution across the jet was found to be decreasing with cylindrical radius unless the mass flow is concentrated in the innermost flux surfaces.

The shape of the magnetosonic surfaces of the wind flow (the position of the critical points along each flux surface) was found to collimate asymptotically into a cylinder. This result is different to that of e.g. self-similar calculations by other authors. It indicates that the asymptotic jet is structured dynamically perpendicular to the jet axis. This would presumably have some influence on the magnetohydrodynamic stability of the asymptotic jet.

Acknowledgements. This work was partly supported by the Deutsche Forschungsgemeinschaft (DFG) and by the Swedish Natural Science Research Council (NFR).

Appendix A: wind polynomial coefficients

Here we list the five coefficients of the cold wind Eq. (21). Although there is a difference in the normalization of the flux tube function $\Phi(x)$, the coefficients A_m are written in a way similar to those given by Camenzind (1986),

$$
\begin{aligned}
A_0 &= x^2(1-x^2)^2 - E^2 x^2 (1-x^2)(1-x_\mathrm{A}^2)^2 ,\\
A_1 &= -2 g x^4 (1 - x^2 - E^2 (1-x_\mathrm{A}^2)^2) ,\\
A_2 &= g^2 x^4 (x^2 - E^2 (x^2 - x_\mathrm{A}^4)) + x^2 (1-x^2)^2 ,\\
A_3 &= -2 g x^4 (1-x^2) ,\\
A_4 &= g^2 x^6 .
\end{aligned}
$$

Here, $g \equiv (\Phi\sigma)^{-1}$.

Appendix B: numerical techniques

B.1. Scan of the magnetic structure

The magnetic field distribution as a solution to the GSS equation is calculated using the method of finite elements (see paper I). For a solution $\Psi(x,z)$, each flux surface $\Psi_n(x,z)$ = const. can be expressed as a 1D function $z = z(x;\Psi_n)$. The same holds for the gradient of Ψ (i.e. the poloidal magnetic field).

The wind equation is a 1D equation along the flux surface. Therefore we have to *scan* the distribution $\Psi(x,z)$ for each of the chosen values of the flux function Ψ_n and the corresponding gradients. Because we applied finite elements of the serendipity class, which are curvilinear and of second order, two problems enter the numerical procedure: First, the non–rectangular shape of the elements implies that the transformation of the calculated solution,

$$\Psi(x,z) = \sum_{i=1}^{8} \Psi_i^e N_i(\xi,\eta) , \tag{B1}$$

is not just straightforward. Instead, a system of the two equations

$$\sum_{i=1}^{8} x_i^e N_i(\xi,\eta) - x = 0 , \quad \sum_{i=1}^{8} \Psi_i^e N_i(\xi,\eta) - \Psi = 0 \tag{B2}$$

has to be solved for the unknown rectangular coordinates on the normalized element, ξ and η. The indices i and (e) mark the solution at the knot i of the element e. The N_i are certain shape functions (see paper I, and references therein). With the solution (ξ,η) for a chosen (x,Ψ),

$$z = \sum_{i=1}^{8} z_i^e N_i(\xi,\eta) = z(x;\Psi) , \tag{B3}$$

and

$$\nabla\Psi = \sum_{i=1}^{8} \Psi_i^e \nabla N_i(\xi,\eta) = \nabla\Psi(x;\Psi) . \tag{B4}$$

can be calculated.

Secondly, because of the use of finite elements of the serendipity class of second order, the gradients are not always continuous between the elements. The 2nd order is, of course, well enough for describing the derivatives within the element. But the 8 nodal points of each element only allow for Ψ as variable on the element knots, not for $\nabla\Psi$. Therefore, in the case of steep gradients the flux tube function has to be splined.

B.2. Determination of the critical solution

In order to find the critical solution of the cold wind equation, i.e. that single solution, smoothly passing the magnetosonic point with magnetosonic speed, we apply a bracketing method. In this approach, the topology of the solutions around the critical point is investigated numerically and the total energy parameter $E(\Psi)$ is varied until the critical solution is found. Depending of the flow parameters and the field structure the wind solution u_P looks quite different: Sub–critical solutions with $E > E_\mathrm{cr}$ do not reach the critical point nor the asymptotic radius. Supercritical solutions do not reach the critical point. They do not continue from the injection radius to the asymptotic radius. Our bracketing procedure investigates all these different possible characteristics of the solution, and improves the parameter E according to the critical condition.

As it was found, for a low magnetization the critical energy has to be determined within an accuracy of $\lesssim 10^{-9}$, sometimes involving complications with the numerical precision of

the computer of 10^{-16}. While the latter problem is due to the relativistic treatment (differences of small numbers), the high precision for the energy parameter is also required in a Newtonian description.

B.3. Numerical tests

Numerical tests were provided by analytical solutions of the cold wind equation. These can be derived e.g. under the assumption of a monopole topology of the magnetic field (Michel 1969).

Additionally, the wind polynomial can be simplified at the LC. Since the coefficients A_0 and A_3 vanish, Eq.(21) reduces to

$$u_{\rm P}^3 + u_{\rm P}\,(1 - E^2(1 - x_{\rm A}^4)) + 2\,E^2(1 - x_{\rm A}^2)^2\,\Phi\,\sigma = 0\,. \qquad \text{(B5)}$$

This equation can be solved analytically (e.g. applying Cardans's solution of the cubic). A similar calculation can be done at the Alfvén radius.

References

Appl, S., Camenzind, M., 1992, A&A, 256, 354
Blandford, R.D., Payne, D.G., 1982, MNRAS, 199, 883
Böhm, K.-J., Solf, J., 1994, ApJ, 430, 277
Camenzind, M., 1986, A&A, 162, 32
Camenzind, M., 1987, A&A, 184, 341
Camenzind, M., 1990, Magnetized disk–winds and the origin of bipolar outflows, in: Klare, G. (ed) Rev. Mod. Astron., 3, Springer, Heidelberg, p. 234
Contopoulos, J., Lovelace, R.V.E., 1994, ApJ, 429, 139
Contopoulos, J., 1994, ApJ, 432, 508
D'Odorico, S., Oosterloo, T., Zwitter, T., Calvani, M., 1991, Nature, 353, 329
Fendt, C., 1994, PhD thesis, University of Heidelberg
Fendt, C., Camenzind, M., Appl, S., 1995, A&A, 300, 791 (paper I)
Ferreira, J., Pelletier, G., 1995, A&A, 295, 807
Goldreich, P., Julian, W.H., 1970, ApJ, 160, 971
Hartigan, P., Morse, J., Heathcote, S., Cecil, G., 1993, ApJ, 414, L121
Kennel, C.F., Fujimura, F.S., Okamoto, I., 1983, J. Ap. Geophys. Fluid Dyn., 26, 147
Kundt, W., 1993, The bipolar outflow phenomenon, in: Errico, L., Vittone, A. (eds) Stellar Jets and Bipolar Outflows, Kluwer Academic Publishers, Dordrecht, p. 51
Kwan, J., Tademaru, E., 1988, ApJ, 332, L41
Li, Z., 1993a, PhD thesis, University of Colorado, Boulder
Li, Z., 1993b, ApJ, 415, 118
Michel, F.C., 1969, ApJ, 158, 727
Mirabel, I.F., Rodriguez, L.F., 1994, Nature, 371, L46
Mundt, R., Brugel, E.W., Bührke, T., 1987, ApJ, 319, 275
Mundt, R., Ray, T.P., Bührke, T., Raga, A.C., Solf, J., 1990, A&A, 232, 37
Okamoto, I., 1978, MNRAS, 173, 357
Paatz, G., Camenzind, M., 1995, A&A, in press
Pelletier, G., Pudritz, R., 1992, ApJ, 394, 117
Pudritz, R., Norman, C.A., 1983, ApJ, 274, 677
Raymond, J., Morse, J., Hartigan, P., Curiel, S., Heathcote, S., 1994, ApJ, 434, 232
Rosso, F., Pelletier, G., 1994, A&A, 287, 325
Sakurai, N.I., 1985, A&A, 152, 121
Sakurai, N.I., 1987, PASJ, 39, 821
Sauty, C., Tsinganos, K., 1994, A&A, 287, 893
Solf, J., 1987, A&A, 184, 322
Tingay, S.J., Jauncey, D.L., Preston, R.A., Reynolds, J.E., Meier, D.L., Murphy, D.W., Tzioumis, A.K., McKay, D.J., Kesteven, M.J., Lowell, J.E.J., Campell-Wilson, D., Ellinsson, S.P., Gough, R., Hunstead, R.W., Jones, J.L., McCulloch, P.M., Migenes, V., Quick, J., Sinclair, M.W., Smits, D., 1995, Nature, 374, 141
Tsinganos, K., Sauty, C., 1992, A&A, 257, 790
Weber, E.J., Davis, L., 1967, ApJ, 148, 217

This article was processed by the author using Springer-Verlag LaTeX A&A style file version 3.